

Original Research

Inulae Flos is a potential herbal medicine to treat glioma: a study based on gene expression profile analysis, network pharmacology and molecular docking

Qian Ying[#], Yi Fang^{#*}

Department of Oncology, Yichang Central People's Hospital, The First College of Clinical Medical Science, China Three Gorges University & Tumor Prevention and Treatment Center of three Gorges University & Cancer Research Institute of three Gorges University, Yichang 443003, China

[#]Qian Ying and Yi Fang contributed equally to this work

*Correspondence to: Yi Fang, 3288785378@qq.com

Abstract: Inulae Flos is a promising herbal medicine; however, its underlying mechanism in treating glioma remains unclear. This study aimed to elucidate the potential active ingredients and mechanisms of Inulae Flos in glioma treatment. Differentially expressed genes (DEGs) associated with gliomas were identified by analyzing the GSE186057 dataset. The bioactive components of Inulae Flos were searched in the Traditional Chinese Medicine Systems Pharmacology database, and related targets were obtained from the Swiss Target Prediction database. A protein-protein interaction (PPI) network was constructed using the STRING database. Next, the Gene Ontology (GO) and Kyoto Encyclopedia of Genes and Genomes (KEGG) of these common targets were analyzed using the DAVID database. Finally, AutoDock Vina was used for molecular docking analysis. The tumor-suppressive properties of the crude extract of Inulae Flos (XFH) and britanin were then evaluated with in vitro and in vivo assays. Nineteen active ingredients were obtained from Inulae Flos, and 20 DEGs were identified as the targets of Inulae Flos in glioma treatment. Britanin, luteolin and 1-O-Acetylbritannilactone were identified as the key ingredients. PIK3R1, CDK2, CCNB1, MAPK1, MAPK8, CCNA2, and AR were considered to be the hub target genes of Inulae Flos in glioma treatment. Good binding affinity was observed between the key components and hub targets. In addition, in vitro studies showed that XFH and britanin, a key component of Inulae Flos, could inhibit the growth, migration and invasion glioma cell lines U87 and U138, and repress the tumorigenesis of U138 cells in nude mice. Inulae Flos is promising for glioma treatment, and it exerts its anti-tumor activities via multiple components, targets and pathways.

Keywords: Inulae Flos, Glioma, Network pharmacology, Molecular docking

Introduction

Glioma accounts for approximately 25% of primary central nervous system tumors, with an average mortality rate of 4.43 per 100,000 persons. Its prognosis is extremely poor, especially for glioblastoma multiforme (GBM) [1-4]. Currently, surgical resection combined with

radiotherapy and temozolomide (TMZ) chemotherapy is the main treatment strategy for gliomas [5]. However, the patients' prognosis remains unsatisfactory [6]. Therefore, there is an urgent need to develop novel anticancer drugs for glioma treatment.

Inulae Flos (Xuanfuhua in Chinese) is a perennial herb belonging to the Asteraceae family and the genus *Inula*. It is widely distributed in Asia, Africa and Europe

Received: May 21, 2024; Revised: Oct.16, 2024; Accepted: Oct.30, 2024; Published: Nov.12, 2024

Copyright © 2024 Qian Ying, Yi Fang.

DOI: <https://doi.org/10.55976/dt.32024132232-52>

This is an open-access article distributed under a CC BY license (Creative Commons Attribution 4.0 International License)

<https://creativecommons.org/licenses/by/4.0/>

and is commonly used in traditional Chinese medicine (TCM) [7]. In China, its is often used to treat digestive diseases, bronchitis, and some inflammatory diseases [8, 9]. Modern pharmacological studies have shown that the main bioactive components of Inulae Flos are terpene lactones (e.g., 1,6-O,O-diacetylbritannilactone, 1-O-acetylbritannilactone, neobritannilactone A, and neobritannilactone B) and flavonoids (e.g., luteolin, patuletin, and quercetin) [10]. Inulae Flos extract can reduce mast cell-mediated allergic reactions induced by immunoglobulin E in animal models [11]. Polysaccharides extracted from Inulae Flos show antidiabetic activity in alloxacin-or streptozotocin-induced diabetic mice by protecting β -cells [12, 13]. In addition, Japonicone A, a natural product extracted from Inulae Flos, has significant antitumor activity against breast cancer, non-small cell lung cancer and myeloma [14-16]. However, the potential value of Inulae Flos for glioma treatment remains unclear.

Network pharmacology is a powerful approach that combines system biology, pharmacology, and bioinformatics analysis to predict disease targets and molecular mechanisms of drug [17, 18]. (Figure 1). This study aimed to predict the potential active ingredients and targets of Inulae Flos, and investigate its tumor-suppressive properties on glioma cells, to evaluate its value in glioma treatment.

Materials and methods

Identification and analysis of differentially expressed genes (DEGs) in glioma

From the Gene Expression Omnibus (GEO, <http://www.ncbi.nlm.nih.gov/geo/>), GSE186057 dataset (Platform: Pancancer Pathways Panel, NanoString Technologies, Inc.) [19] was downloaded. This database contains gene expression data of 24 GBM tissue samples and 12 normal tissues (adjacent normal tissue, ANT). Using GEO2R tool (<http://www.ncbi.nlm.nih.gov/geo/geo2r/>), DEGs between tumor and ANT samples were obtained. The thresholds were $P < 0.05$, and $|\log_2\text{fold change}| > 1$, and the results were visualized using volcano and heat maps. The ade4 package in R software was used for principal component analysis (PCA), and the ggplot2 package was used for visualization. The CIBERSORT algorithm was used to analyze the immune cells of GBM and ANT samples in the GSE186057 dataset, and a box diagram was used to visualize the immune cell composition of the two groups of samples. The Wilcoxon rank-sum test was used to evaluate differences in the proportions of immune cells. $P < 0.05$ was considered statistically significant. Gene Ontology (GO) and Kyoto Encyclopedia of Genes and Genomes (KEGG) enrichment analyses of DEGs were performed using the clusterProfiler package in R software.

Screening of bioactive components and targets of Inulae Flos

Based on oral bioavailability (OB) $\geq 30\%$ and drug-likeness (DL) ≥ 0.18 , the active components of Inulae Flos were obtained from the Traditional Chinese Medicine Systems Pharmacology database (TCMSP, <https://www.tcm-sp-e.com/>) [20]. The SMILES files of ingredients were obtained from the PubChem database (<https://pubchem.ncbi.nlm.nih.gov>) and imported into the Swiss Target Prediction database (<http://www.swisstargetprediction.ch>) to obtain the ingredients targets, and the threshold was probability > 0.1 [21].

Construction and analysis of protein-protein interaction (PPI) networks at drug-disease common targets

Common drug-disease targets were imported into the STRING database (<https://cn.string-db.org/>) for PPI analysis [22]. The species was defined as "Homo sapiens" and the required minimum interaction score was set to "medium confidence (0.4)". Topological network analysis was performed using the CytoNCA plug-in in the Cytoscape 3.9.0 software [23]. In addition, the Molecular Complex Detection (MCODE) plug-in was used to perform module analysis of protein targets in the PPI network, according to default parameters [23]. The default parameters were degree cutoff = 2, node score cutoff = 0.2, K-score = 2, and maximum depth = 100.

GO and KEGG pathway analysis of drug-disease common targets

Using the Database for Annotation, Visualization, and Integrated Discovery (DAVID) database (<https://david.ncifcrf.gov/tools.jsp>) [24], common targets of glioma and Inulae Flos were subjected to GO and KEGG enrichment analyses. The species were defined as "Homo sapiens", and $P < 0.05$ was used as the screening condition.

Identification and analysis of hub target genes

Using the CytoHubba plugin in the Cytoscape 3.9.0 software [23], the top 10 key genes in PPI network analysis were calculated using different algorithms, such as betweenness, closeness, degree, maximal clique centrality (MCC), radiality, and stress. The R software UpSet package was used to screen for cross genes, which were considered hub genes.

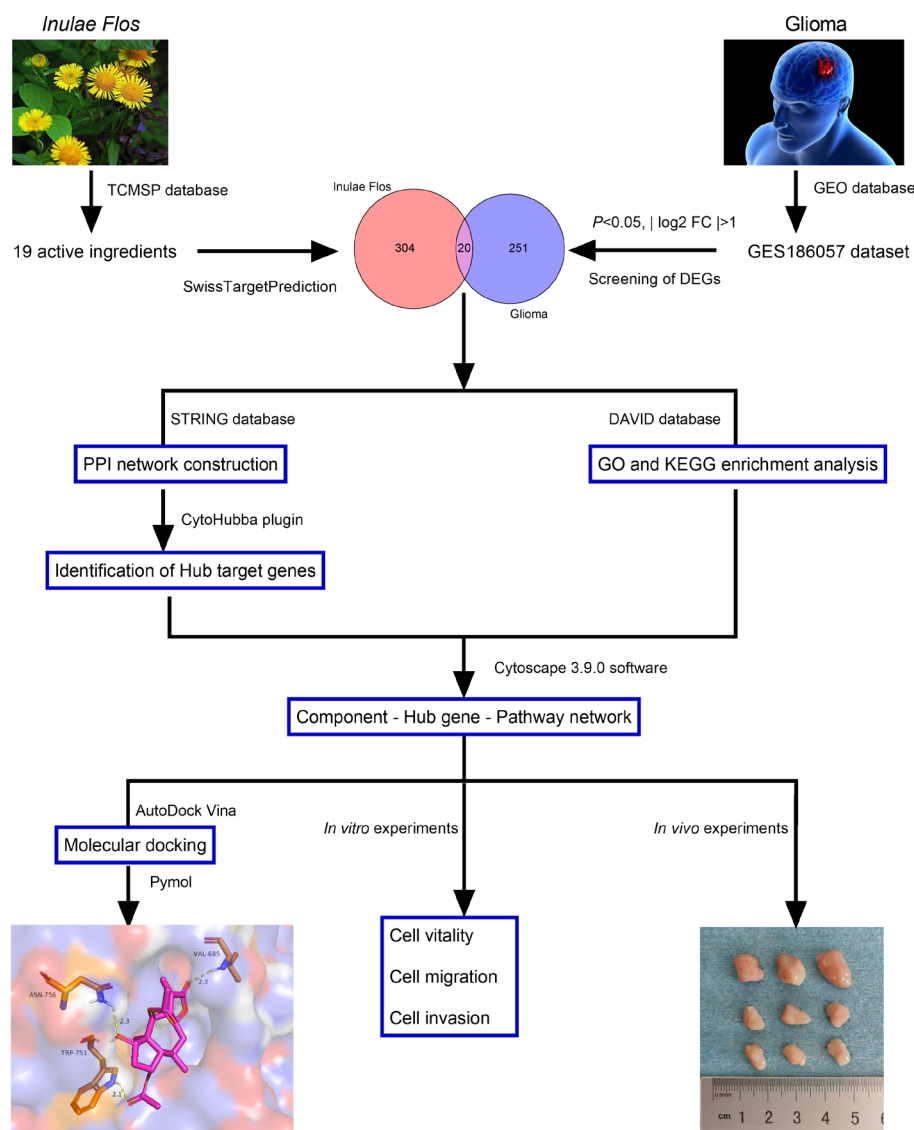


Figure 1. The workflow of the present work

Construction and analysis of "component-hub target gene-pathway" network

The top 10 KEGG terms with the most gene counts were imported into Cytoscape 3.9.0 software to plot the "component-hub gene-pathway" network diagram, and the degree values of network nodes were calculated by CytoNCA plug-in [23], so as to screen out the key components and major hub target genes of *Inulae Flos* in glioma treatment. The expression characteristics of the hub targets in glioma tissues and non-cancerous brain tissues in The Cancer Genome Atlas (TCGA) were analyzed using GEPIA database (<http://gepia.cancer-pku.cn/>) [25].

Molecular docking

Molecular docking analysis was performed using AutoDock Vina (version 1.1.2) to evaluate the ability of key components to bind to major hub targets. The 3D chemical structures of key components were downloaded from PubChem (<https://pubchem.ncbi.nlm.nih.gov/>) and saved in the SDF format. They were then converted to the mol2 format using OpenBabel software (version 3.1.1). From the Protein Data Bank (PDB; <https://www.rcsb.org/>), X-ray crystal structures of the major hub targets were downloaded. All protein receptor and molecular ligand files were converted to pdbqt files using the AutoDockTools software (version 1.5.7). Molecular docking was performed using the AutoDock Vina software [26]. When the binding energy is less than zero, proteins and molecules can spontaneously bind [27]. The PyMOL software was used to visualize the docking results [26].

Cell culture

Human glioma cell lines U87 and U138 were purchased from the American Type Culture Collection (ATCC, Manassas, VA, USA). The cells were placed in a diet containing Dulbecco's Modified Eagle's Medium (DMEM; Invitrogen, Carlsbad, CA, USA) with 10% fetal bovine serum (FBS; Gibco, Carlsbad, CA, USA), 100 U/mL penicillin and 100 µg/mL streptomycin in an incubator containing 5% CO₂ at 37 °C.

Preparation of Inulae Flos extract

For the extraction of Inulae Flos, 40 g Inulae Flos (Qiancao, Xi'an, China) was heated in 500 mL boiling water for 30 min, and then the liquid was collected after filtration. The residue was then heated in 250 mL of boiling water for 30 min, and then the liquid was also collected after filtration. The liquids were mixed, and a freeze drying process was performed to obtain the medicinal powder. The powder was then dissolved in dimethylsulfoxide (DMSO; Beyotime, Shanghai, China), and diluted by the medium, and filtered by 0.22 µm filter twice. The crude extract of Inulae Flos was named as XFH (short for the Chinese name of Inulae Flos, Xuanfuhua).

Cell viability assay

Cell counting Kit 8 (CCK-8; Beyotime, Shanghai, China) was used to detect cell viability. U87 and U138 cells were seeded into 96-well plates at a density of 3×10³ cells per well. After overnight incubation, the cells were treated with XFH (0, 12.5, 25, 50, 100 µg/ml), or britanin (98.0% purity, CAS No. 33627-28-0, Bohu Biotechnology Co., Ltd, Shanghai, China) (0, 1, 3, 5, and 7 µM) for 24 h. Then, 10 µL of CCK-8 was added to each well of the plate and the cells were further incubated for 4 h. Optical density (OD) was measured at 450 nm.

Transwell assay

The migration and invasion abilities of the glioma cells were analyzed by Transwell assay. In the migration experiment, after U87 and U138 cells were treated with XFH (100 µg/ml) or britanin (7 µM) for 24 h, they were re-suspended in 200 µL of serum-free medium and the cell suspension was added into the upper compartment of a Transwell system (8-µm pore size, Corning, NY, USA). The lower compartment was supplemented with 750 µL complete medium. After culturing for 48 h, the cells on the below surface of the membrane were fixed with methanol for 30 min and stained with 0.1% crystal violet for 10 min. After the membrane was washed by tap water to remove the excessive dye, 6 fields were randomly selected under the microscope to observe and count the cells. The invasion experiment was similar, except that the

membrane was pre-coated with a layer of Matrigel (BD Bioscience, San Jose, CA, USA).

In vivo tumorigenesis assay

The Laboratory Animal Ethics Committee of Renmin Hospital of Wuhan University approved the animal experimental procedures in this study (WDY2021K070). A total of 9 6-week-old male nude mice were used (BALB/C, Model Animal Center of Wuhan University, kept in SPF condition with free access to food and water). The nude mice were randomly divided into three groups [blank control group, XFH treatment group, and britanin treatment group, 3 mice in each group]. U138 cells were treated with XFH (100 µg/ml) or britanin (7 µM) for 24h. Then cell suspension was prepared, and the concentration was adjusted to 1 × 10⁸ cells /ml, and the inoculation volume was 0.1 ml. The cell suspension was injected into the subcutaneous tissue of the back of nude mice through a sterile syringe. After injection, the tumor growth was checked regularly. By measuring the length and width of the tumor, the tumor volume was calculated using the formula $V = 1/2 \times \text{length} \times \text{width}$. After 24 days, the nude mice were euthanized, and the tumors were isolated and weighted.

Statistical analysis

For in vitro assays, all experiments were conducted independently in triplicates. All data are expressed as mean ± standard deviation (SD). SPSS (version 21.0; IBM Corp., Armonk, NY, USA) was used for all the statistical analyses. Multivariate comparisons were performed using one-way analysis of variance (ANOVA) and Tukey's post hoc test. $P < 0.05$ was considered statistically significant.

Results

Identification and analysis of DEGs in glioma

GSE186057 was used to identify the DEGs in GBM. PCA showed significant differences between GBM and ANT tissue samples (Figure 2A). Notably, 271 DEGs, including 123 upregulated and 148 downregulated genes, were found between GBM and ANT tissues (Figures 2B, C; Table 1). The CIBERSORT algorithm was used to calculate the proportion of 22 types of immune cells in GBM and ANT samples (Figures 3A and B). Compared with ANT, the infiltration of B cells memory, naive B cells naive, macrophages M0, macrophages M2, Mast cells activated, resting mast cells resting, plasma cells and T cells CD4 memory activated were reduced in GBM tissues, while the infiltration of neutrophils, T cells CD4 memory resting, T cells, CD8 T cells, and

gamma delta T cells was increased (Figure 3C). GO and KEGG enrichment analyses were performed to study the biological functions and mechanisms of these DEGs. GO analysis showed that these DEGs were mainly enriched in peptidyl-tyrosine phosphorylation, peptidyl-tyrosine modification, regulation of MAP kinase activity, regulation of peptidyl-tyrosine phosphorylation, and epithelial cell proliferation (Figure 3D). KEGG analysis showed that 182 pathways were associated with DEGs (P

< 0.05). The top 10 pathways with the lowest P value were the MAPK signaling pathway (hsa04010), Ras signaling pathway (hsa04014), breast cancer (hsa05224), PI3K-Akt signaling pathway (hsa04151), gastric cancer (hsa05226), human papillomavirus infection (hsa05165), melanoma (hsa05218), Rap1 signaling pathway (hsa04015), acute myeloid leukemia (hsa05221), and proteoglycans in cancer (hsa05205) (Figure 3E).

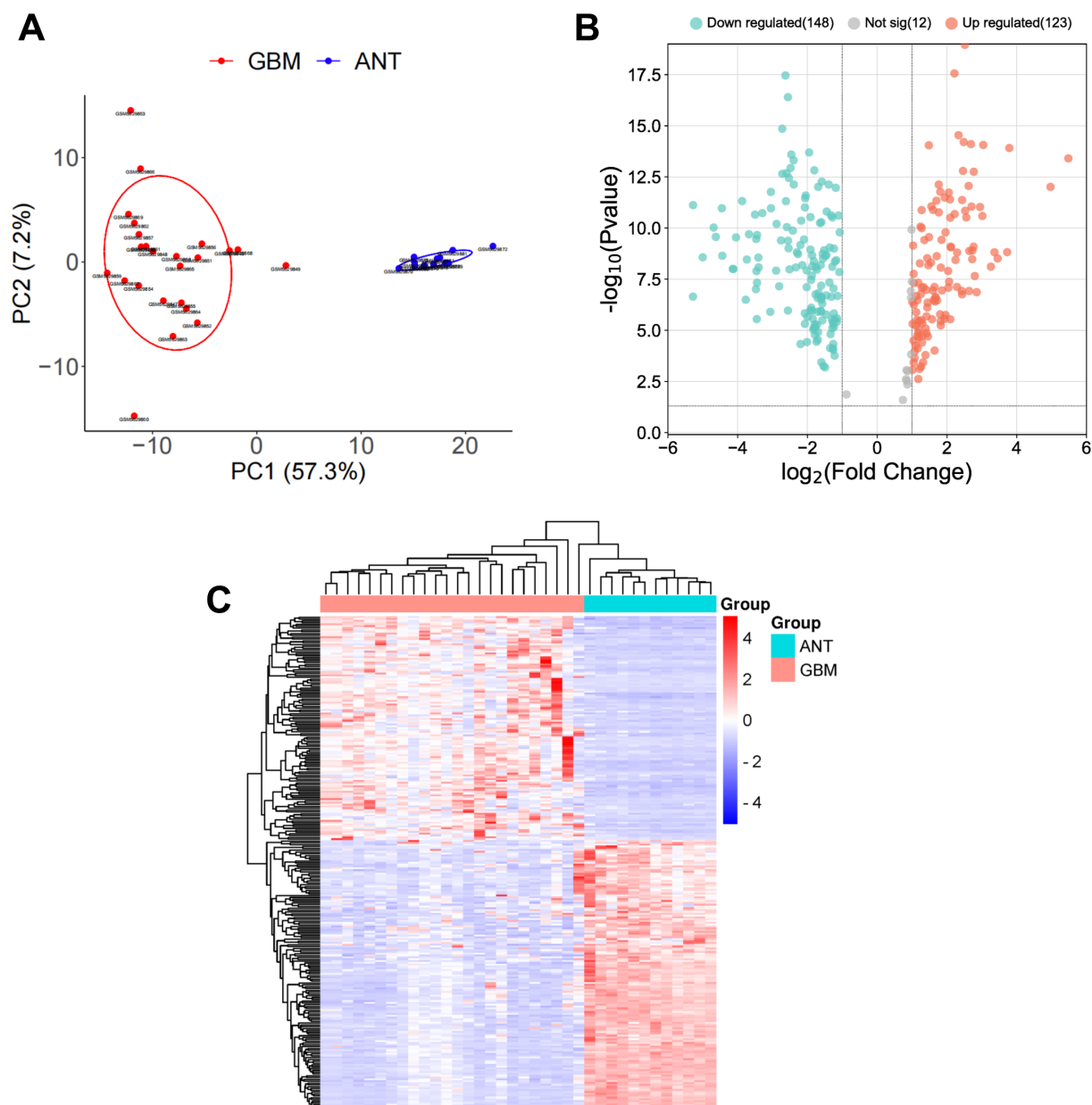


Figure 2. Identification of DEGs in glioma

A.PCA diagram of GSE186057; B. The expression patterns of the DEGs are shown in a volcano map. Red and blue dots represent upregulated genes ($\log_2\text{FC} > 1$) and downregulated genes ($\log_2\text{FC} < -1$), respectively. Gray dots represent genes with no significant difference in expression; C.Heat map of DEGs in GBM and ANT tissues.

Table 1. Screening DEGs in glioma

DEGs	Gene symbol
Upregulated gene	TP53, MYD88, MCM7, BRCA2, NOTCH1, CDK2, SP1, TNC, HIST1H3B, MYC, LAMA5, BRCA1, EIF4EBP1, HIST1H3G, PLCE1, TCF7L1, CHEK1, SMO, POLD1, IKBKB, FANCC, FLNA, WEE1, STAT3, RELA, TNFRSF10B, MCM5, EZH2, MCM2, CDKN2C, GADD45A, ATM, PDGFC, ITGA7, TCF3, PML, IDH1, ABL1, RUNX1, NOTCH3, JAG1, ITGB4, HIST1H3H, VEGFA, CLCF1, CCNA2, PCNA, MAML2, SOCS3, ITGB3, HSPB1, BLM, HDAC1, MAP3K1, HSPA6, NUPR1, PIM1, ARID2, FLNC, TTK, FANCE, MUTYH, TLR2, RAD51, HELLS, EPHA2, BAX, CASP8, SPRY4, HES1, PLAUI, CD14, SPP1, H3F3A, LFNG, H2AFX, DDB2, WNT5A, MFNG, MAP3K14, PKMYT1, FGF11, CDC25B, COL27A1, HSP90B1, TGFB1, PBX3, CDC25C, FZD7, LAMB4, HSPA1A, GADD45B, ETV4, MAD2L2, PIK3R5, BRIP1, IL6R, B2M, FANCG, CCND1, RASA4, CCNB1, FANCA, CHEK2, PGF, PRKX, SHC1, RAC2, FAS, POLE2, DLL4, ERBB2, ID1, CDK6, SPRY2, AR, LEF1, IL1RAP, GNG12, IL2RB, SOCS1, SPRY1, DLL1
Downregulated gene	MAPK9, PPP3R1, FBXW7, MAPK1, PPP3CA, PRKACB, DUSP8, MAP2K4, STAT4, PRKAR2B, AKT3, LIG4, PPP3CB, SKP1, MAPK3, NF1, COL24A1, PRKAA2, PPP2R2B, PRKCB, CACNB4, WIF1, MAPK8, PRKCG, CACNB2, ACVR2A, FGF12, WNT10B, PRKACA, BRAF, MAP2K1, PPP2R1A, MAPK10, BNIP3, TIAM1, PRKAR1B, CCNA1, PTPRR, TSPAN7, TBL1XR1, IL12RB2, BDNF, RASGRF1, NPM2, CACNA1E, PPP3R2, RASGRF2, SHC3, EFNA3, PIK3R1, CHAD, SIRT4, CACNA1C, HDAC11, PLCB1, FIGF, STMN1, PLA2G4E, MPL, GRIN2B, CALML3, RELN, PRMT8, RNF43, GRIN2A, FUT8, ARNT2, MSH2, FGFR2, CACNA2D1, FGF16, MAP3K13, CDKN2D, PAK3, RASGRP1, PPP2R2C, RASAL1, MAPT, RUNX1T1, WNT2, ACVR1C, FGF13, ACVR1B, GATA1, MPO, FGF21, PAK7, FGF22, CAMK2B, MAPK8IP2, FANCL, MAPK8IP1, IL23R, FGF4, DKK4, WNT2B, GRIN1, WNT10A, RPS6KA5, CALML5, PRKACG, IL22RA2, CACNA2D3, FGF23, NTRK2, CACNA1D, CACNA2D2, MRE11A, DKK2, PAX8, COL6A6, FGF14, RPS6KA6, FZD3, IFNA2, KIT, PLA2G4C, PITX2, PTPN5, PLA1A, PLA2G4F, CREB3L3, LEFTY1, FASLG, FGF20, FGF9, HSPA2, FLT3, CCNO, FGF10, FGF5, PPARGC1A, WNT16, EFNA5, DUSP2, SMC1B, TPO, TNF, BAIAP3, KLF4, FGF7, HNF1A, MGMT, FGF8, CBLC, FGF17, FGFR3, LRP2

Note. DEGs, differentially expressed genes.

Screening of active constituents and their targets of Inulae Flos

According to $OB \geq 30\%$ and $DL \geq 0.18$, 19 potentially active components were obtained from the TCMSP database. Basic information of the active ingredients is provided in Table 2. Subsequently, the targets of these active ingredients were predicted using the Swiss Target Prediction database and 324 drug targets were identified after merging and deleting duplicate candidates.

Construction and analysis of PPI network for drug-disease common targets

To obtain the target of Inulae Flos in glioma treatment, 20 common targets were obtained from the 324 drug targets and 271 DEGs mentioned above (Figure 4A). These 20

common drug-disease targets were then imported into the STRING database for PPI network construction. As shown (Figure 4B), a PPI network with 20 nodes and 57 edges was constructed. The average node degree of the network was 5.7 and the average local clustering coefficient was 0.495. Furthermore, the topological parameters of the PPI network were analyzed, and all nodes were arranged in a circle according to the degree value, which was proportional to the size of the node and the shade of the color (Figure 4C). In addition, module analysis of the PPI network was performed, resulting in a subnetwork of 7 nodes and 19 edges (score = 6.333, Figure 4D).

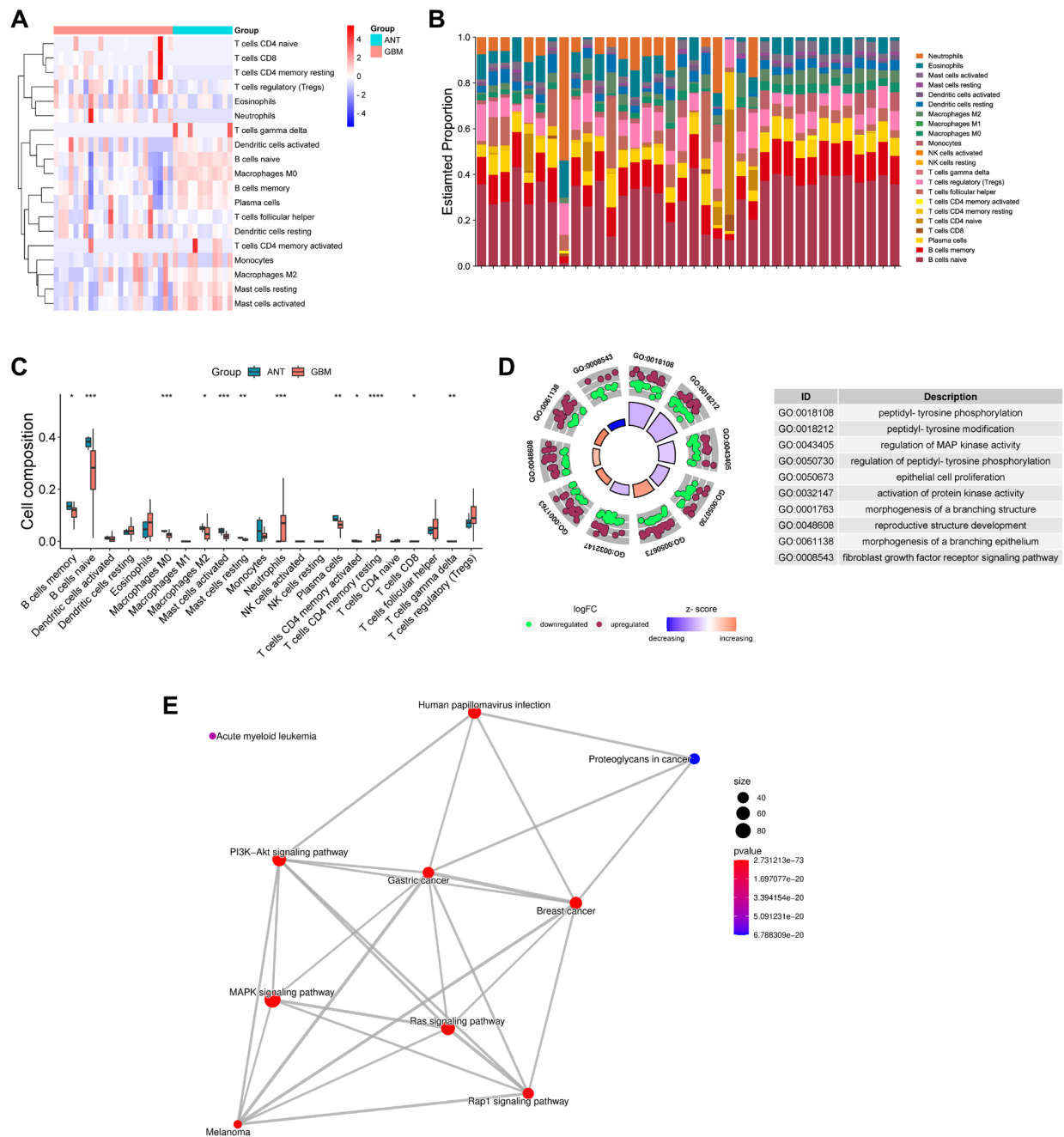
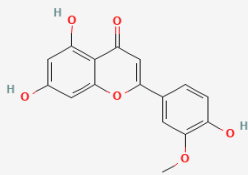
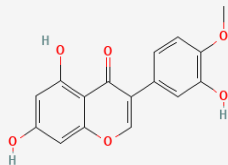
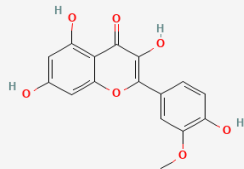
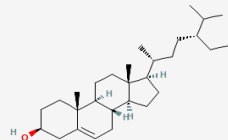
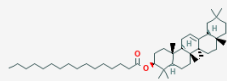
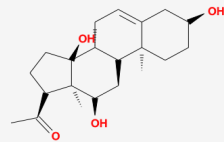
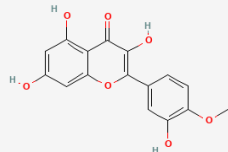
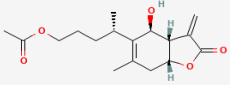
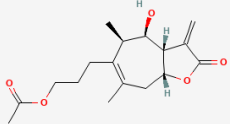
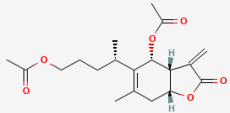
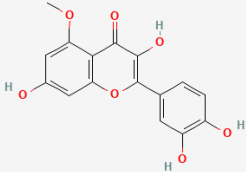
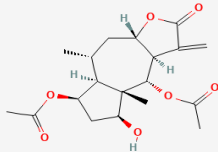
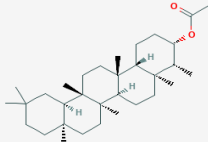
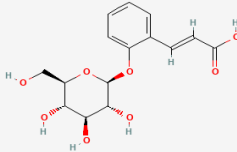


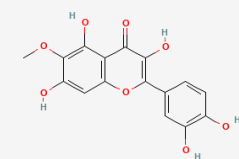
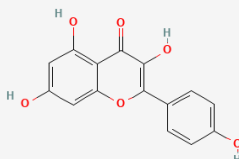
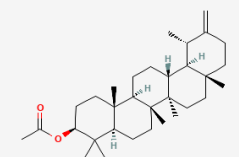
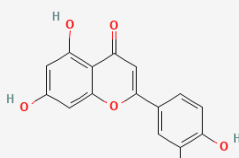
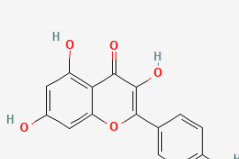
Figure 3. Immunoinfiltration in glioma and enrichment analysis of DEGs

A and B. CIBERSORT algorithms were used to detect scale maps (A) and heat maps (B) of 22 immune cells in GBM and ANT tissue samples; C. Comparison of each type of immune cell between GBM and ATC tissues.; D. The top 10 GO-BP enrichment terms with the most significant P values; E. Emapplot of enriched pathways. *P < 0.05, **P < 0.01, ***P < 0.001.

Table 2. Details of active compounds in Inulae Flos

Mol ID	Molecule Name	OB (%)	DL	Target	Pubchem Cid	Molecular structure
MOL003044	Chryseriol	35.85	0.27	103	5280666	
MOL003398	Pratensein	39.06	0.28	60	5281803	
MOL000354	Isorhamnetin	49.6	0.31	103	5281654	
MOL000358	Beta-Sitosterol	36.91	0.75	44	222284	
MOL000363	beta-Amyrin palmitate	32.68	0.3	2	13915599	
MOL003851	Isoramanone	39.97	0.51	N/A	N/A	
MOL004083	Tamarixetin	32.86	0.31	103	5281699	

Mol ID	Molecule Name	OB (%)	DL	Target	Pubchem Cid	Molecular structure
MOL004089	1-O-Acetylbritannilactone	30.12	0.22	109	75528891	
MOL004090	DTXSID00955263	73.35	0.22	111	442263	
MOL004092	1,6-O,O-diacetylbritannilactone	39.03	0.31	1	10360513	
MOL004093	Azaleatin	54.28	0.3	103	5281604	
MOL004094	Britanin	33.73	0.41	105	5315501	
MOL004096	Epifriedelanol acetate	31.18	0.74	15	13688752	
MOL004101	Melilotoside	36.85	0.26	8	5280759	

Mol ID	Molecule Name	OB (%)	DL	Target	Pubchem Cid	Molecular structure
MOL004112	Patuletin	53.11	0.34	103	5281678	
MOL000422	Kaempferol	41.88	0.24	103	5280863	
MOL000596	Taraxasterol acetate	43.08	0.74	19	13889352	
MOL000006	Luteolin	36.16	0.25	103	5280445	
MOL000098	Quercetin	46.43	0.28	103	5280343	

Note. OB, oral bioavailability; DL, drug-likeness.

GO and KEGG enrichment analyses of drug-disease common targets

To further explore the mechanism of *Inulae Flos* in glioma treatment, GO and KEGG enrichment analyses were performed based on common drug–disease targets. GO analysis revealed a total of 85 GO terms, including 60 biological processes (BP), 9 cell components (CC), and 16 molecular functions (MF). The top 10 BP, CC, and MF terms with the highest gene counts were selected for visualization. As shown (Figure 4A), BP was

mainly associated with protein phosphorylation, signal transduction, positive regulation of transcription, DNA templated, G2/M transition of the mitotic cell cycle, and peptidyl-serine phosphorylation. CC was mainly associated with the cytosol, nucleus, nucleoplasm, cytoplasm, and plasma membrane (Figure 5A). MF was associated with protein binding, protein serine/threonine/tyrosine kinase activity, ATP-binding protein serine/threonine kinase activity, and protein kinase activity (Figure 5A). In KEGG enrichment analysis, 104 pathways were identified. The top 10 predicted pathways with the highest gene counts are shown, including pathways in cancer (hsa05200),

the MAPK signaling pathway (hsa04010), acute myeloid leukemia (hsa05221), and myeloid leukemia (hsa05221). progesterone-mediated oocyte maturation (hsa04914), cellular senescence (hsa04218), human T-cell leukemia virus 1 infection (hsa05166), microRNAs in cancer (hsa05206), hepatitis B (hsa05161), human immunodeficiency virus 1 infection (hsa05170), and the Ras signaling pathway (hsa04014) (Figure 5B). The top 20 KEGG pathways with the highest gene counts were classified. These KEGG pathways were divided into four main categories: environmental information processing,

cellular processes, organismal systems, and human diseases (Figure 5C). In addition, secondary classification of all KEGG pathways was performed (Figure 5D). These pathways were mainly related to signal transduction, cell growth and death, eukaryote cellular community, transport, and catabolism.

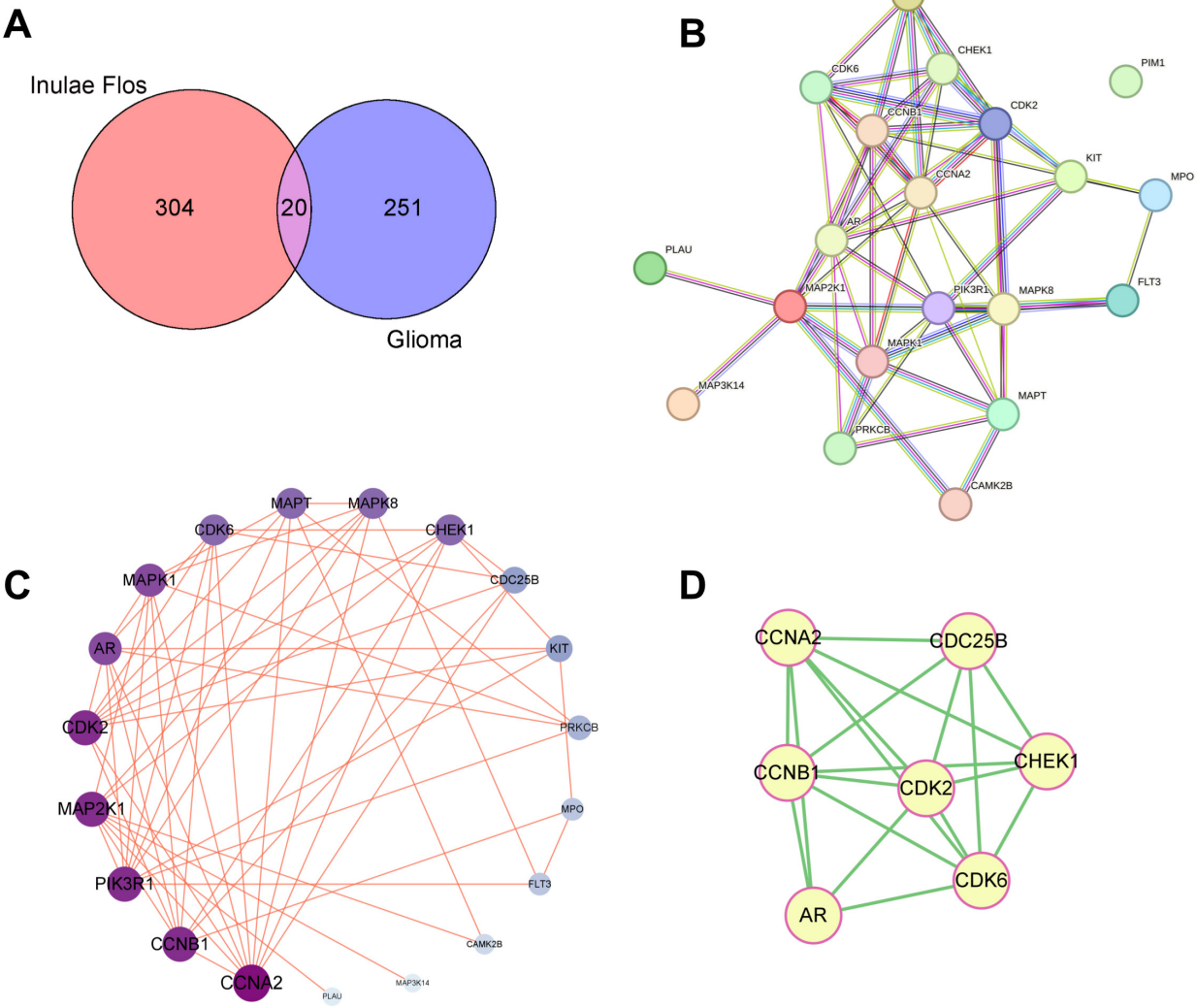


Figure 4. PPI network analysis of the targets of Inulae Flos for glioma treatment

A. Venn diagram is used to screen out the shared genes from target genes of Inulae Flos and DEGs in glioma; B. PPI network of the common genes. Nodes represent proteins and edges represent protein-protein interactions; C. CytoNCA plug-in is used to calculate the degree values of the PPI network nodes. The larger the degree value, the larger the node; D. MCODE plug-in is used to screen highly interconnected clusters in PPI network. MCODE score = 6.333.

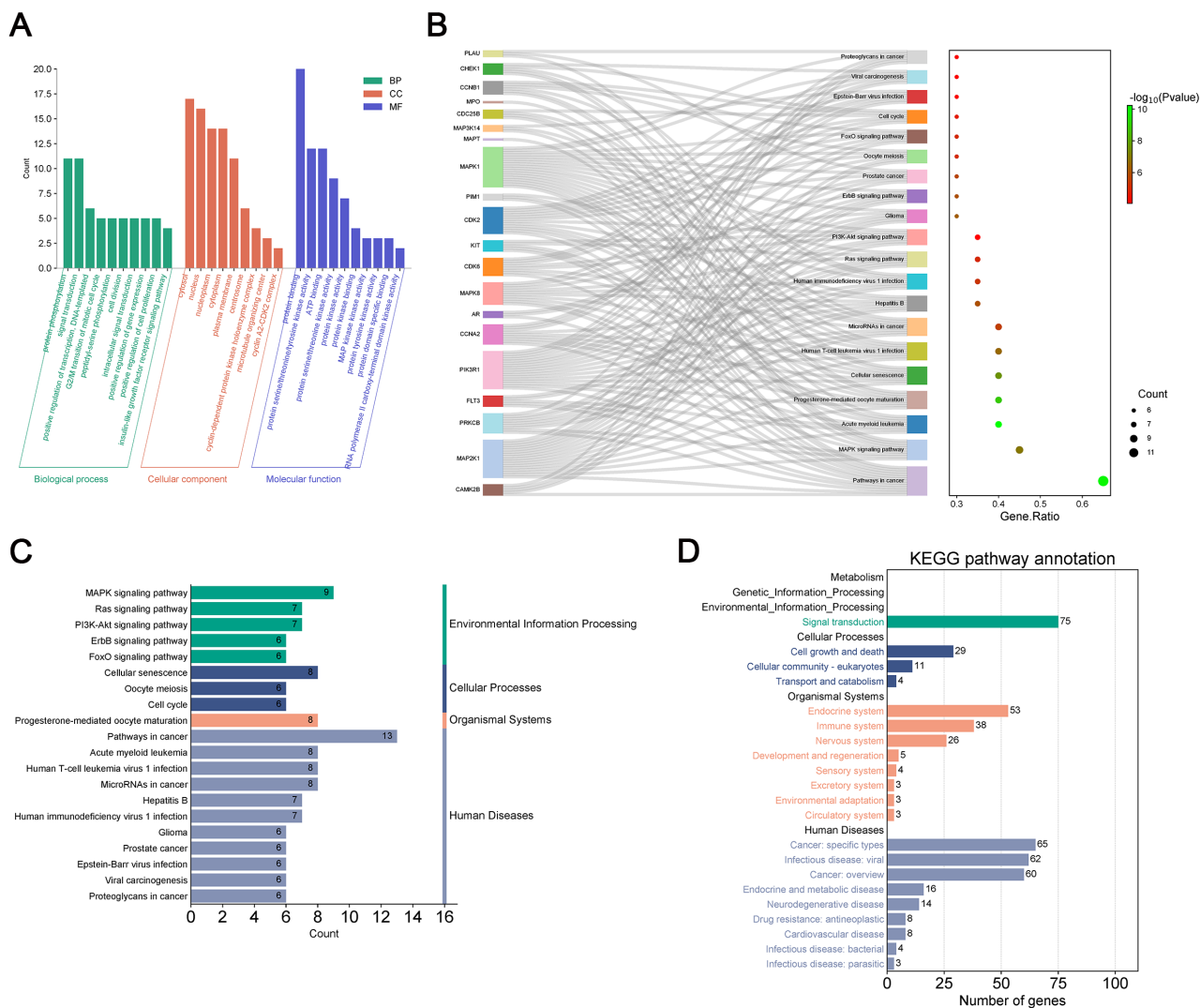


Figure 5. GO and KEGG enrichment analysis of the targets of Inulae Flos for glioma treatment

A. Histogram of the top 10 biological processes (green), cell components (red), molecular functions (blue) associated with Inulae Flos with the most gene counts ($P < 0.05$); B. Sankey and bubble maps of the top 20 KEGG pathways with the most gene counts. On the left side of the diagram is the sankey diagram, which represents the genes contained in each pathway. On the right is the bubble map, the size of the bubble represents the gene count, and the color of the bubble represents the P-value; C. Classification diagram of the top 20 KEGG channels; D. Secondary classification diagram of all KEGG channels.

Table 3. The top 10 target gene rank in CytoHubba

Rank	Betweenness	Closeness	Degree	MCC	Radiality	Stress
1	MAP2K1	CCNA2	CCNA2	CCNA2	CCNA2	MAP2K1
2	PIK3R1	PIK3R1	PIK3R1	CCNB1	PIK3R1	PIK3R1
3	CCNB1	CCNB1	CCNB1	CDK2	CCNB1	CCNA2
4	CCNA2	MAP2K1	MAP2K1	CDK6	MAP2K1	CCNB1
5	MAPT	CDK2	CDK2	CHEK1	MAPK1	MAPT
6	CDK2	MAPK1	AR	CDC25B	MAPK8	CDK2
7	MAPK8	AR	MAPK1	MAPK1	CDK2	MAPK1
8	MAPK1	MAPK8	CDK6	AR	CHEK1	AR
9	AR	CHEK1	MAPK8	MAPK8	AR	MAPK8
10	CHEK1	CDK6	MAPT	PIK3R1	CDK6	CHEK1

Table 4. Hub target information of Inulae Flos in the treatment of glioma

Gene	Uniprot ID	Description	Betweenness	Closeness	Degree	MCC	Radiality	Stress
PIK3R1	P27986	phosphoinositide-3-kinase regulatory subunit 1	37.42106227	13.5	9	30	2.722222222	112
CDK2	P24941	cyclin dependent kinase 2	16.11483516	13.16666667	9	154	2.611111111	60
CCNB1	P14635	cyclin B1	33.03388278	13.5	9	163	2.722222222	86
MAPK1	P28482	mitogen-activated protein kinase 1	12.96947497	13	8	48	2.666666667	54
MAPK8	P45983	mitogen-activated protein kinase 8	15.86904762	12.5	7	32	2.611111111	48
CCNA2	P20248	cyclin A2	22.21312576	14	10	180	2.777777778	92
AR	P10275	androgen receptor	11.92478632	12.5	8	42	2.5	50

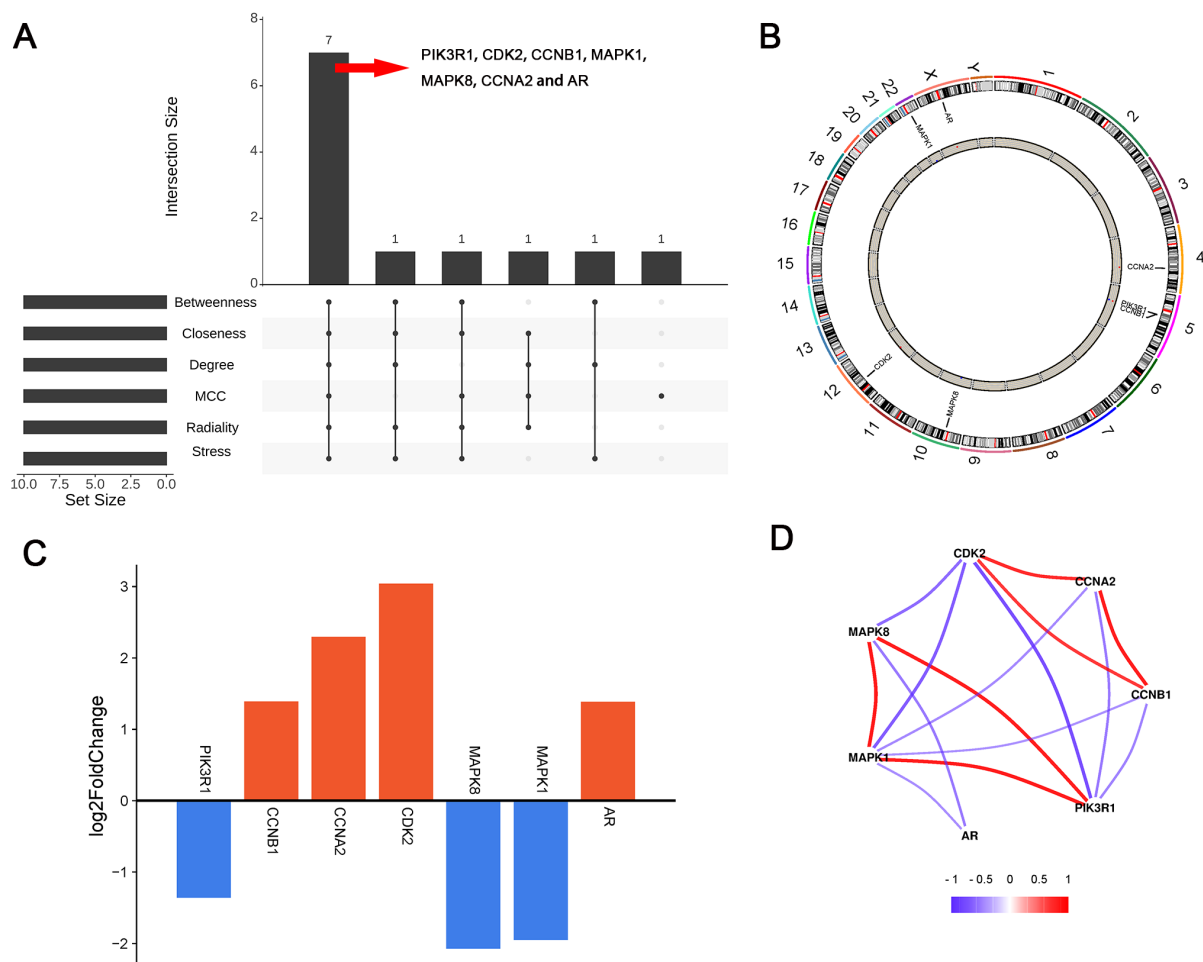


Figure 6. Identification of hub target gene in treatment of glioma by Inulae Flos

A. The upset map of Betweenness, closeness, degree, MCC, radiality and stress algorithms; B. Circos graph is generated using the Circos package in R software. The outer layer of the Circos diagram shows chromosome positions, and the inner layer represents the differentially expressed hub genes; C. Histogram is used to map the differential expression of hub gene in GBM and ANT tissues. The X-axis is the gene, and the Y-axis is the change fold. Red means up-regulated, above the X-axis; Blue is down-regulated, below the X-axis; D. Correlation coefficient network of the hub genes' expression in GBM tissues. The larger the correlation coefficient, the thicker the line. Blue indicates a negative correlation and red indicates a positive correlation.

Construction of "component-hub target gene-pathway" network

Subsequently, the bioactive components of *Inulae Flos*, the hub target genes and top 10 pathways with most gene counts were imported into Cytoscape 3.9.0 to construct the "component-hub target gene-pathway" network. The network consisted of 32 nodes and 104 edges (Figure 7A). In this network, the five hub genes with the highest degree values were PIK3R1 (degree value = 17), CDK2 (degree value = 15), CCNB1 (degree value = 14), MAPK1 (degree value = 13), and MAPK8 (degree value = 8). The three active ingredients with the highest degree values were britanin (degree value = 7), luteolin (degree value = 5), and 1-O-Acetylbritannilactone (degree value = 5) (Figure 7B). The expression characteristics of the 5 potential targets and AR, CCNA2, were also investigated with the data from TCGA, and the results showed that compared with non-cancerous brain tissues, the expression of CDK2, CCNB1, CCNA2 and AR was highly expressed in GBM tissues, however the expression of PIK3R1, MAPK1 and MAPK8 was not remarkably changed (Figure 7C-I).

Molecular docking of key components and major hub genes

In order to explore the interaction between active components of *Inulae Flos* and predicted hub targets, 3 key components (britanin, luteolin, and 1-O-Acetylbritannilactone) and 5 major hub targets (PIK3R1, CDK2, CCNB1, MAPK1, and MAPK8) were selected for molecular pairing. Binding energies less than 0 kcal/mol indicate possible binding between two molecules, and binding energies less than -5.0 kcal/mol indicate strong binding activity between molecules [27, 28]. The results showed that britanin, luteolin, and 1-O-Acetylbritannilactone had good binding affinities for the five targets (Figure 8A-E). The docking results implied that the role of *Inulae Flos* in glioma treatment was dependent on multiple components and targets.

XFH and britanin inhibited growth and aggressiveness of glioma cells

To verify the potential function of *Inulae Flos* in glioma treatment, the crude extract of *Inulae Flos* (XFH) was used to treat glioma cells in vitro. Britanin, a key component of *Inulae Flos*, was also selected to treat the cells. U87 and U138 cells were treated with different concentrations of XFH (0, 12.5, 25, 50, 100 µg/ml) or britanin (0, 1, 3, 5, and 7 µM) for 24 h and cell viability was determined using the CCK-8 method. As shown (Figure 9A-D), XFH and britanin exhibited significant anti-growth activity in both the U87 and U138 cells in a concentration-dependent manner. Transwell assay showed that XFH (100 µg/ml) and britanin (7 µM) respectively repressed the migration and invasion abilities of U87 and U138 cells (Figure 9E-J).

Additionally, after U138 cells were treated with XFH (100 µg/ml) or britanin (7 µM), the tumorigenesis ability in nude mice was significantly reduced (Figure 10). These data further support the hypothesis that *Inulae Flos* and britanin have tumor-suppressive properties for gliomas.

Discussion

Using a dataset of gene expression profiles, 271 DEGs (GBM tissues vs. ANT) were identified in the present study. Bioinformatic analysis suggested that these DEGs play a key role in multiple biological processes and pathways. Our findings suggest that the pathological mechanisms underlying gliomas are complex. Therefore, there is a need to develop novel treatment strategies that can modulate multiple targets and pathways in gliomas to improve the patients' prognosis. Herbal medicines consist of multiple bioactive components that may exert pharmacological effects [29-32]. In recent years, TCM has shown great value in the treatment of glioma [30-32]. For example, extracts of *Curcumae Longae Rhizoma* and *Crocus sativus* L. can inhibit the malignant biological behaviors of gliomas by regulating the immune-inflammatory response [31, 32]. Previous studies have shown that *Inulae Flos* has multiple pharmacological effects, including anti-tumor effects [10-16]. However, to the best of our knowledge, its pharmacological mechanism for treating glioma has not yet been studied. In the present work, it was observed that the crude extract of *Inulae Flos* has significant tumor-suppressive effects on glioma cells.

Through network pharmacological analysis, we identified three key components of *Inulae Flos*, britanin, luteolin, and 1-O-Acetylbritannilactone, which can interact with multiple targets. Britanin, a sesquiterpene lactone compound, has significant antioxidant and anti-inflammatory activities [33]. Britanin has significant anti-proliferative activity against human prostate carcinoma, gastric carcinoma, pancreatic carcinoma, and triple-negative breast carcinoma [33-36], and in the present work, in vitro and in vivo assays have also supported that britanin represses the growth of glioma cells. Luteolin (3,4,5,7-tetrahydroxy flavone) is a flavonoid found in various plants including vegetables, herbs, and fruits. In vitro and in vivo studies suggest that it can be used as an anticancer agent against various types of human malignancies such as lung carcinoma, breast carcinoma, GBM, prostate carcinoma, colonic carcinoma, and pancreatic carcinoma [37]. There is evidence that 1-O-Acetylbritannilactone has a variety of biological effects, including anti-inflammatory, anti-bacterial, anti-hepatitis, anti-diabetes, and anti-tumor effects [38-40]. Together with these reports, our findings suggest that *Inulae Flos* may block glioma progression via britanin, luteolin, and 1-O-Acetylbritannilactone.

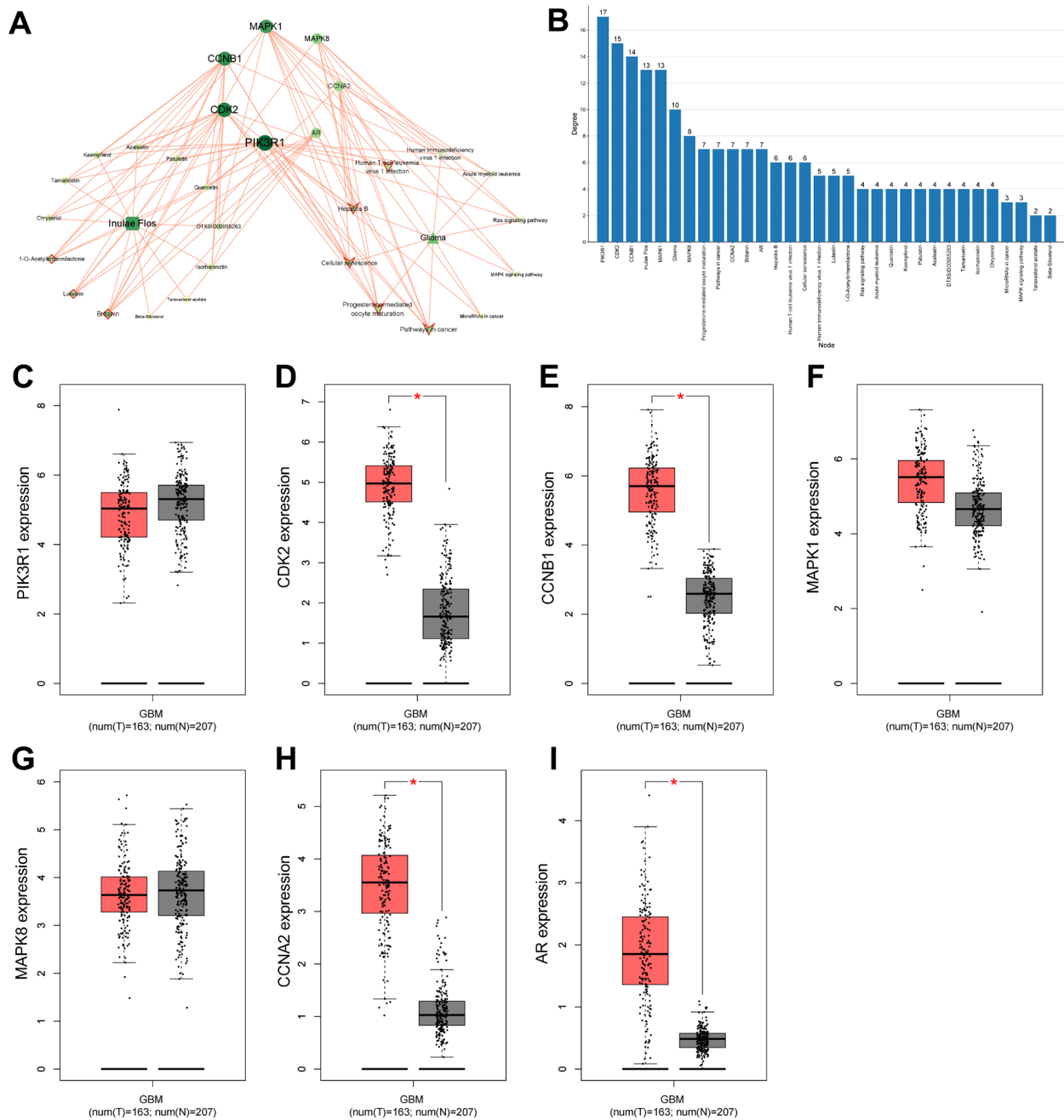


Figure 7. Construction of the "component-hub target gene-pathway" network

A. Construction of the "component-Hub target gene-pathway" network using Cytoscape 3.9.0 software. A V-shaped node represents a pathway; a circular node represents a target; triangular node represents glioma; a diamond node represents a component; square node represents Inulae Flos. The node size or color shade is proportional to the magnitude of the degree value; B. Bar chart of degree value statistics of the "component -hub target gene-pathway" network; C-I. The expression levels of PIK3R1 (C), CDK2 (D), CCNB1 (E), MAPK1 (F), MAPK8 (G), CCNA2 (H), AR (I) in GBM tissues and non-cancerous brains tissues were analyzed using GEPIA database.

* $P < 0.001$.

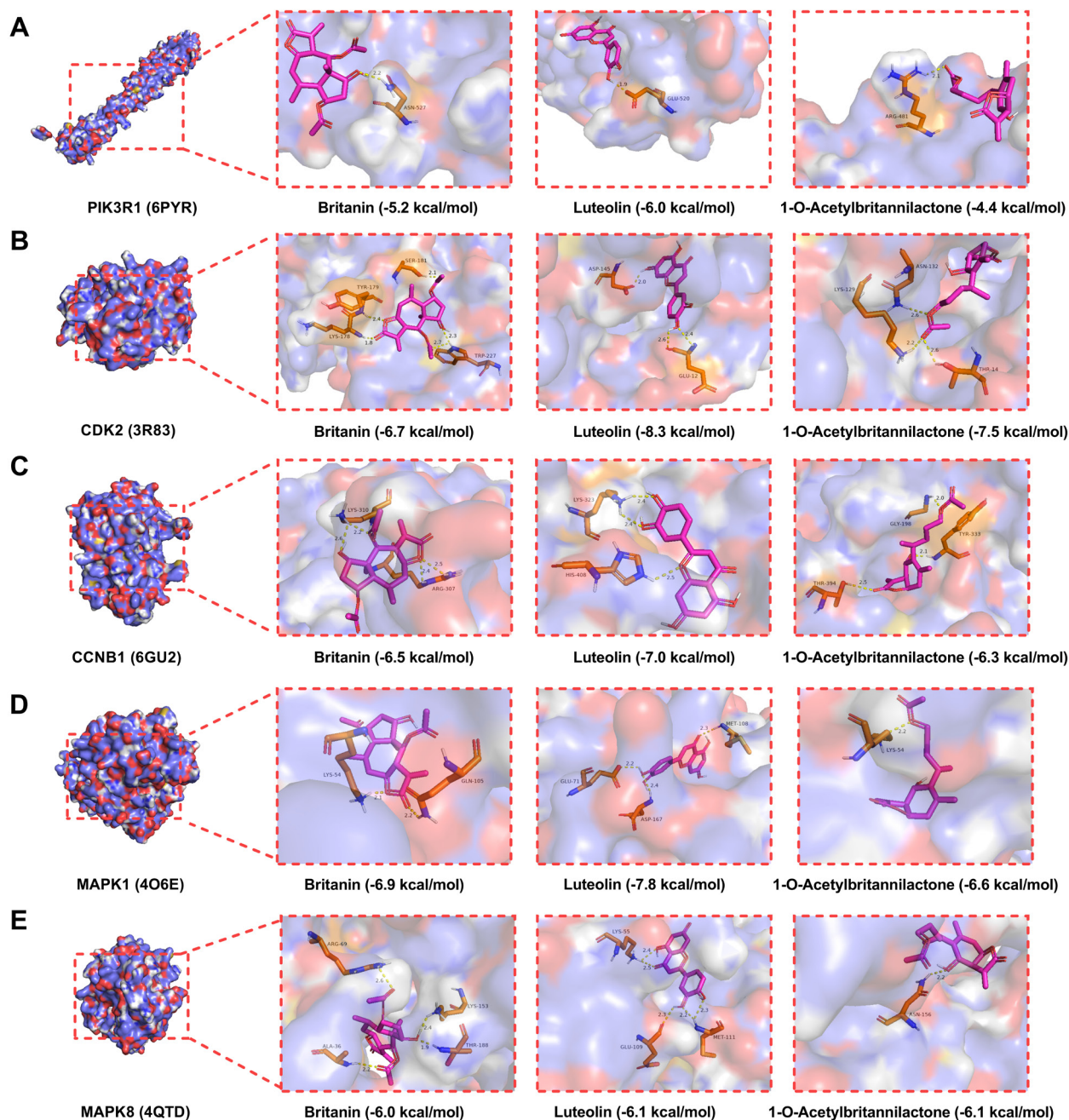


Figure 8. 3D molecular docking diagram of key components and hub targets

A-E. Molecular docking diagram of key components britanin, luteolin, 1-O-Acetylbritannilactone and major hub targets PIK3R1 (A), CDK2 (B), CCNB1 (C), MAPK1 (D), MAPK8 (E). Purple represents key components (ligands), orange represents amino acid residues surrounding the binding bag, and yellow dashed lines represent hydrogen bonds.

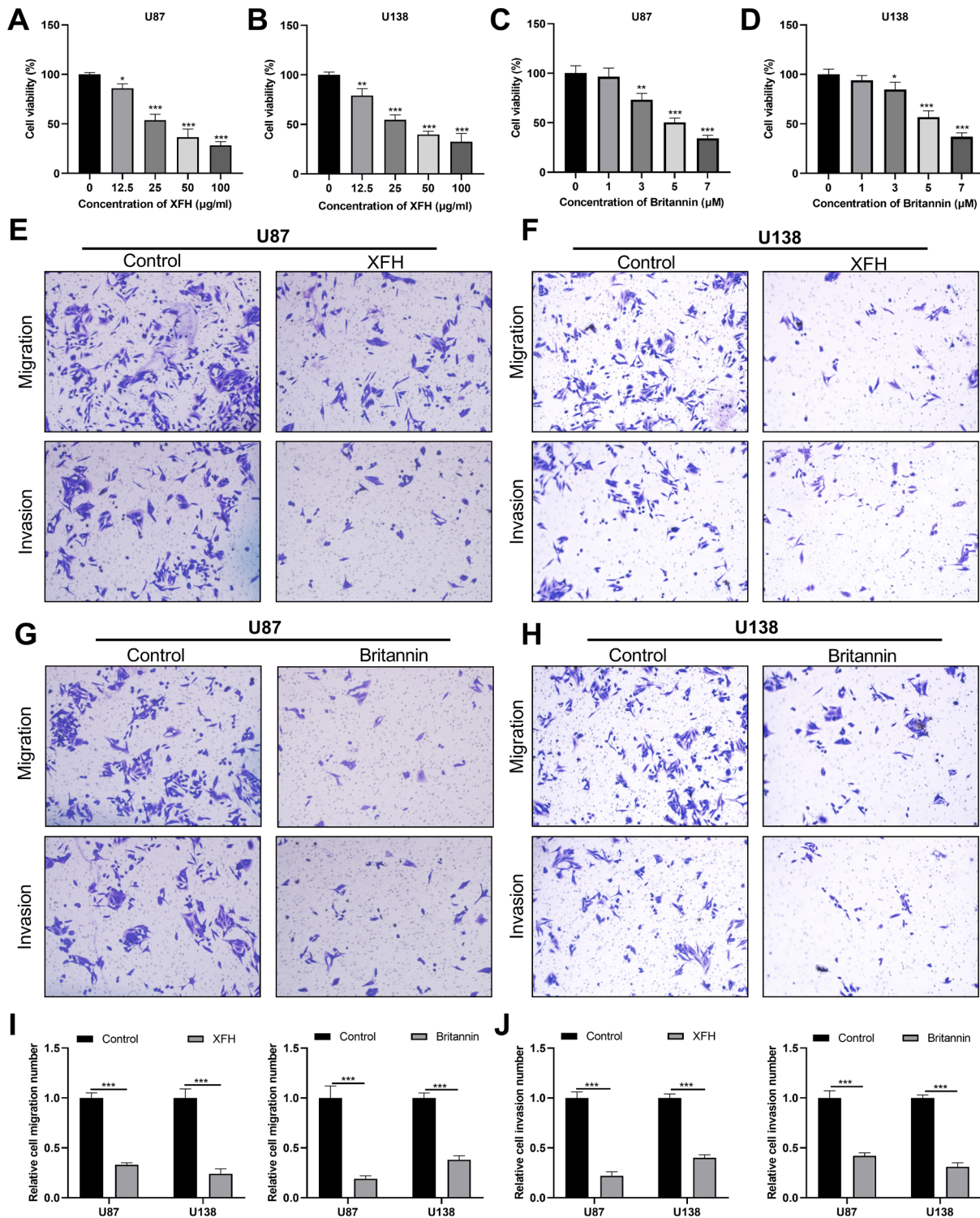


Figure 9. Crude extract of *Inulae Flos* and britanin inhibited the viability and aggressiveness of glioma cells

A-B. CCK-8 assay was used to evaluate the effects of different concentrations of XFH (0, 12.5, 25, 50, 100 μg/ml) on the viability of the U87 (A) and U138 (B) cells; C-D. CCK-8 assay was used to evaluate the effects of different concentrations of Britannin (0, 1, 3, 5, and 7 μM) on the viability of the U87 (C) and U138 (D) cells; E-F. A-B. CCK-8 assay was used to evaluate the effects of 100 μg/ml XFH on the migration ability and invasion ability of the U87 (A) and U138 (B) cells; G-H. A-B. CCK-8 assay was used to evaluate the effects of 7 μM Britannin on the migration ability and invasion ability of the U87 (G) and U138 (H) cells; I-J. The quantitative results of Transwell assays. **P < 0.01, ***P < 0.001, compared with the control group.

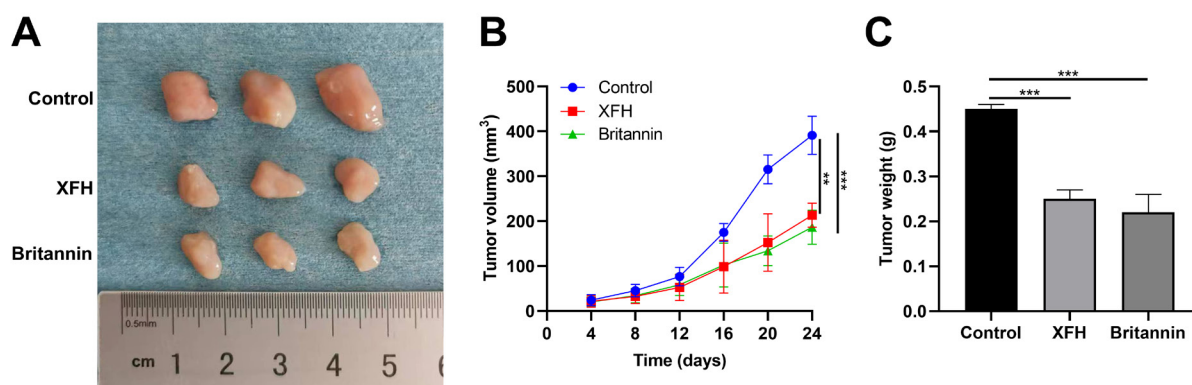


Figure 10. XFH and Britannin inhibited the growth of glioma cells in vivo

A. U138 cells were inoculated into the subcutaneous tissues of nude mice. This figure shows the tumors in control group, XFH treatment group, and britannin treatment group; B. The tumor volume of the mouse in each group was measured every 4 days; C. The weights of the tumor in each group were measured and compared. ** $P < 0.01$, *** $P < 0.001$, compared with the control group.

Our study reported that PIK3R1, CDK2, CCNB1, MAPK1, MAPK8, CCNA2, and AR, with high topological parameters, were hub targets of Inulae Flos in the treatment of glioma. We also analyzed the GES186057 dataset and found that PIK3R1, MAPK1, and MAPK8 were downregulated, whereas CDK2, CCNB1, CCNA2, and AR were upregulated in GBM tissues. A previous study reported that the expression of PIK3R1 is low in glioma and its high expression is associated with good prognosis in glioma patients [41], which is consistent with our findings. In addition, CDK2, CCNB1, CCNA2, and AR have been reported to be overexpressed in gliomas and are associated with poor patient prognosis[42-44], which is consistent with our findings. MAPK1 knockdown can inhibit the phosphorylation of its downstream proteins, thereby inhibiting the proliferation of glioma cells and inducing apoptosis [45]. MAPK8 is upregulated in TMZ-resistant GBM cells, which promotes resistance to TMZ of cancer cells by activating the MAPK signaling pathway, accelerates cell proliferation, and inhibiting cell apoptosis [46]. In our work, molecular docking showed that the 5 major hub targets (5 major hub targets (PIK3R1, CDK2, CCNB1, MAPK1, and MAPK8)) have good binding affinity to britannin, luteolin, and 1-O-Acetylbritannilactone, which suggests that Inulae Flos may suppress the proliferation, aggressiveness and chemoresistance of glioma cells via these hub targets.

KEGG analysis showed that the treatment of glioma by Inulae Flos involved multiple pathways, including the MAPK, Ras, and PI3K-Akt signaling pathways. The MAPK signaling pathway plays a key role in supporting tumor survival and proliferation [45-47]. The Ras signaling pathway is an important part of the cell signaling pathway and plays a crucial role in carcinogenic signaling [48]. The PI3K-Akt signaling pathway is closely associated with the progression of various cancers, and targeting the PI3K-Akt signaling pathway is a promising strategy for glioma treatment [49]. However, the regulatory effects of Inulae

Flos and its functional components on these pathways remain to be investigated in molecular biological studies.

It is necessary to claim that because the completeness of the databases used in this work is uncertain, some components and targets may be missed, and more open-access databases and more diverse omics data will be helpful to further clarify the role of Inulae Flos and its targets in glioma treatment[50]. What's more, based on molecular docking the binding affinity between the components of Inulae Flos and the hub targets, should be further validated with techniques such as molecular dynamics simulation[51]. Additionally, the blood-brain barrier permeability of the active components including britannin, should be carefully considered in future studies, which is crucial for clinical applications, and the safety and efficacy require more data from clinical trials.

Conclusion

Inulae Flos may play an important role in the treatment of glioma by acting on multiple targets and pathways via multiple bioactive components. Our findings provide crucial information regarding the pharmaceutical values of Inulae Flos, and suggest that the bioactive components of Inulae Flos, including britannin, are promising candidate drugs for clinical treatment of glioma.

Authors' contribution

All authors made a significant contribution to the work reported, whether that is in the conception, study design, execution, acquisition of data, analysis and interpretation, or in all these areas; took part in drafting, revising or critically reviewing the article; gave final approval of the version to be published; have agreed on the journal to which

the article has been submitted; and agree to be accountable for all aspects of the work.

Ethical approval

The use of human data in the present study is exempt from ethical approval, which was permitted by the Research Ethics Committee of Yichang Central People's Hospital, because related bioinformatics analyses did not disclose the patient's privacy, and as ex post analyses, the analyses did not change the procedures of diagnosis and treatment. The Laboratory Animal Ethics Committee of Renmin Hospital of Wuhan University approved all experiments with animals in this study (WDRY2021K070).

Acknowledgement

We thank Dr. Zhou Youdong, from Renmin Hospital of Wuhan University, for his kind support for animal experiments.

Funding information

This study is not supported by any funding agencies. This study is financially supported by the corresponding authors Zhang Haiquan & Zhu Yaozu.

Data availability statement

The data used to support the findings of this study are available from the corresponding author upon request.

References

- [1] Luo H, Zhang H, Mao J, Cao H, Tao Y, Zhao G, Zhang Z, Zhang N, Liu Z, Zhang J, Luo P, Xia Y, Cheng Y, Xie Z, Cheng Q, Liu G. Exosome-based nanoimmunotherapy targeting TAMs, a promising strategy for glioma. *Cell Death Dis.* 2023 Apr 3;14(4):235. doi: 10.1038/s41419-023-05753-9.
- [2] Yang K, Wu Z, Zhang H, Zhang N, Wu W, Wang Z, Dai Z, Zhang X, Zhang L, Peng Y, Ye W, Zeng W, Liu Z, Cheng Q. Glioma targeted therapy: insight into future of molecular approaches. *Mol Cancer.* 2022 Feb 8;21(1):39. doi: 10.1186/s12943-022-01513-z.
- [3] Ostrom QT, Cioffi G, Gittleman H, Patil N, Waite K, Kruchko C, Barnholtz-Sloan JS. CBTRUS Statistical Report: Primary Brain and Other Central Nervous System Tumors Diagnosed in the United States in 2012-2016. *Neuro Oncol.* 2019 Nov 1;21(Suppl 5):v1-v100. doi: 10.1093/neuonc/noac202.
- [4] Mitchell D, Shireman JM, Dey M. Surgical Neuro-Oncology: Management of Glioma. *Neurol Clin.* 2022 May;40(2):437-453. doi: 10.1016/j.ncl.2021.11.003.
- [5] Huang Q, Pan X, Zhu W, Zhao W, Xu H, Hu K. Natural Products for the Immunotherapy of Glioma. *Nutrients.* 2023 Jun 19;15(12):2795. doi: 10.3390/nu15122795.
- [6] Jackson CM, Choi J, Lim M. Mechanisms of immunotherapy resistance: lessons from glioblastoma. *Nat Immunol.* 2019 Sep;20(9):1100-1109. doi: 10.1038/s41590-019-0433-y.
- [7] Park SH, Lee DH, Kim MJ, Ahn J, Jang YJ, Ha TY, Jung CH. Inula Japonica Thunb. Flower Ethanol Extract Improves Obesity and Exercise Endurance in Mice Fed A High-Fat Diet. *Nutrients.* 2018 Dec 20;11(1):17. doi: 10.3390/nu11010017.
- [8] Khan AL, Hussain J, Hamayun M, Gilani SA, Ahmad S, Rehman G, Kim YH, Kang SM, Lee IJ. Secondary metabolites from Inula britannica L. and their biological activities. *Molecules.* 2010 Mar 10;15(3):1562-77. doi: 10.3390/molecules15031562.
- [9] Lu Y, Li X, Park YN, Kwon O, Piao D, Chang YC, Kim CH, Lee E, Son JK, Chang HW. Britanin Suppresses IgE/Ag-Induced Mast Cell Activation by Inhibiting the Syk Pathway. *Biomol Ther (Seoul).* 2014 May;22(3):193-9. doi: 10.4062/biomolther.2014.038.
- [10] Kim YS, Lee JH, Song J, Kim H. Gastroprotective Effects of Inulae Flos on HCl/Ethanol-Induced Gastric Ulcers in Rats. *Molecules.* 2020 Nov 29;25(23):5623. doi: 10.3390/molecules25235623.
- [11] Lu Y, Li Y, Jin M, Yang JH, Li X, Chao GH, Park HH, Park YN, Son JK, Lee E, Chang HW. Inula japonica extract inhibits mast cell-mediated allergic reaction and mast cell activation. *J Ethnopharmacol.* 2012 Aug 30;143(1):151-7. doi: 10.1016/j.jep.2012.06.015.
- [12] Shan JJ, Zhang Y, Diao YL, Qu WS, Zhao XN. Effect of an antidiabetic polysaccharide from Inula japonica on constipation in normal and two models of experimental constipated mice. *Phytother Res.* 2010 Nov;24(11):1734-8. doi: 10.1002/ptr.3212.
- [13] Zhao C, Diao Y, Wang C, Qu W, Zhao X, Ma H, Shan J, Sun G. Structural characters and protecting β -cells of a polysaccharide from flowers of Inula japonica. *Int J Biol Macromol.* 2017 Aug;101:16-23. doi: 10.1016/j.ijbiomac.2017.03.044.
- [14] Feng J, Hu J, Xia Y. Identification of RAD54 homolog B as a promising therapeutic target for breast cancer. *Oncol Lett.* 2019 Nov;18(5):5350-5362. doi: 10.3892/ol.2019.10854.
- [15] Du Y, Gong J, Tian X, Yan X, Guo T, Huang M, Zhang B, Hu X, Liu H, Wang Y, Li J, Li M. Japonicone A inhibits the growth of non-small cell lung cancer cells via mitochondria-mediated pathways. *Tumour Biol.* 2015 Sep;36(10):7473-82. doi: 10.1007/s13277-015-3439-6.
- [16] Zhang Z, Ye C, Liu J, Xu W, Wu C, Yu Q, Xu X, Zeng X, Jin H, Wu Y, Yan H. Japonicone A induces

- apoptosis of bortezomib-sensitive and -resistant myeloma cells in vitro and in vivo by targeting IKK. *Cancer Biol Med*. 2021 Sep 28;19(5):651–68. doi: 10.20892/j.issn.2095-3941.2020.0473.
- [17] Hopkins AL. Network pharmacology: the next paradigm in drug discovery. *Nat Chem Biol*. 2008 Nov;4(11):682-90. doi: <https://doi.org/10.1038/nchembio.118>.
- [18] Liu Z, Huang H, Yu Y, Li L, Shi X, Wang F. Exploring the mechanism of ellagic acid against gastric cancer based on bioinformatics analysis and network pharmacology. *J Cell Mol Med*. 2023 Oct 4. doi: 10.1111/jcmm.17967
- [19] Morrison C, Weterings E, Mahadevan D, Sanan A, Weinand M, Stea B. Expression Levels of RAD51 Inversely Correlate with Survival of Glioblastoma Patients. *Cancers (Basel)*. 2021 Oct 26;13(21):5358. doi: 10.3390/cancers13215358.
- [20] Ru J, Li P, Wang J, Zhou W, Li B, Huang C, Li P, Guo Z, Tao W, Yang Y, Xu X, Li Y, Wang Y, Yang L. TCMSPP: a database of systems pharmacology for drug discovery from herbal medicines. *J Cheminform*. 2014 Apr 16;6:13. doi: 10.1186/1758-2946-6-13.
- [21] Daina A, Michielin O, Zoete V. SwissTargetPrediction: updated data and new features for efficient prediction of protein targets of small molecules. *Nucleic Acids Res*. 2019 Jul 2;47(W1):W357-W364. doi: 10.1093/nar/gkz382.
- [22] Szklarczyk D, Kirsch R, Koutrouli M, Nastou K, Mehryary F, Hachilif R, Gable AL, Fang T, Doncheva NT, Pyysalo S, Bork P, Jensen LJ, von Mering C. The STRING database in 2023: protein-protein association networks and functional enrichment analyses for any sequenced genome of interest. *Nucleic Acids Res*. 2023 Jan 6;51(D1):D638-D646. doi: 10.1093/nar/gkac1000.
- [23] Tang Y, Li M, Wang J, Pan Y, Wu FX. CytoNCA: a cytoscape plugin for centrality analysis and evaluation of protein interaction networks. *Biosystems*. 2015 Jan;127:67-72. doi: 10.1016/j.biosystems.2014.11.005.
- [24] Sherman BT, Hao M, Qiu J, Jiao X, Baseler MW, Lane HC, Imamichi T, Chang W. DAVID: a web server for functional enrichment analysis and functional annotation of gene lists (2021 update). *Nucleic Acids Res*. 2022 Jul 5;50(W1):W216-W221. doi: 10.1093/nar/gkac194.
- [25] Tang Z, Li C, Kang B, Gao G, Li C, Zhang Z. GEPIA: a web server for cancer and normal gene expression profiling and interactive analyses. *Nucleic Acids Res*. 2017 Jul 3;45(W1):W98-W102. doi: 10.1093/nar/gkx247.
- [26] Seeliger D, de Groot BL. Ligand docking and binding site analysis with PyMOL and Autodock/Vina. *J Comput Aided Mol Des*. 2010 May;24(5):417-22. doi: 10.1007/s10822-010-9352-6.
- [27] Luo Z, Xia LY, Tang YQ, Huang L, Liu D, Huai WY, Zhang CJ, Wang YQ, Xie YM, Yin QZ, Chen YH, Zhang TE. Action Mechanism Underlying Improvement Effect of Fuzi Lizhong Decoction on Nonalcoholic Fatty Liver Disease: A Study Based on Network Pharmacology and Molecular Docking. *Evid Based Complement Alternat Med*. 2022 Jan 20;2022:1670014. doi: 10.1155/2022/1670014.
- [28] Li S, Li S, Zhao Q, Huang J, Meng J, Yan W, Wang J, Ren C, Hao L. Mechanisms of Vitamin C Regulating Immune and Inflammation Associated with Neonatal Hypoxic-Ischemic Encephalopathy Based on Network Pharmacology and Molecular Simulation Technology. *Evid Based Complement Alternat Med*. 2022 Feb 14;2022:4904325. doi: 10.1155/2022/4904325.
- [29] Mogwasi R. Bio-Accessibility of Iron and Copper from Seven Kenyan Anti-Anaemia Medicinal Plants. *Diagnostics and Therapeutics*. 2022 Sep; 2(1): 1-12.
- [30] Tan Q, Lu J, Liang J, Zhou Y, Yang C, Zhang Z, Li C. A review of traditional Chinese medicine Curcumae Rhizoma for treatment of glioma. *Int Rev Neurobiol*. 2023;172:303-319. doi: 10.1016/bs.irm.2023.07.004.
- [31] Li H, Li Y. Network Pharmacology Analysis of Molecular Mechanism of Curcuma longa L. Extracts Regulating Glioma Immune Inflammatory Factors: Implications for Precise Cancer Treatment. *Current Topics in Medicinal Chemistry*. 2022 Mar 4;22(4):259-267. doi: 10.2174/1568026621666210910123749.
- [32] Yang X, Man D, Zhao P, Li X. Identification of the therapeutic mechanism of the saffron crocus on glioma through network pharmacology and bioinformatics analysis. *Med Oncol*. 2023 Sep 10;40(10):296. doi: 10.1007/s12032-023-02142-2.
- [33] Zeng Q, Zeng Y, Nie X, Guo Y, Zhan Y. Britanin Exhibits Potential Inhibitory Activity on Human Prostate Cancer Cell Lines Through PI3K/Akt/NF-κB Signaling Pathways. *Planta Med*. 2020 Dec;86(18):1401-1410. doi: 10.1055/a-1211-4656.
- [34] Shi K, Liu X, Du G, Cai X, Zhan Y. In vivo antitumor activity of Britanin against gastric cancer through nuclear factor-κB-mediated immune response. *J Pharm Pharmacol*. 2020 Apr;72(4):607-618. doi: 10.1111/jphp.13230.
- [35] Li K, Zhou Y, Chen Y, Zhou L, Liang J. A novel natural product, britanin, inhibits tumor growth of pancreatic cancer by suppressing nuclear factor-κB activation. *Cancer Chemother Pharmacol*. 2020 Apr;85(4):699-709. doi: 10.1007/s00280-020-04052-w.
- [36] Xu X, Guo Y, Du G, Liu H, Wang L, Chen D. Bioluminescence Imaging-Based Assessment of the Anti-Triple-Negative Breast Cancer and NF-Kappa B Pathway Inhibition Activity of Britanin. *Front Pharmacol*. 2020 May 5;11:575. doi:10.3389/fphar.2020.00575.
- [37] Imran M, Rauf A, Abu-Izneid T, Nadeem M, Shariati MA, Khan IA, Imran A, Orhan IE, Rizwan M, Atif M, Gondal TA, Mubarak MS. Luteolin, a flavonoid, as an anticancer agent: A review. *Biomed Pharmacother*. 2019 Apr;112:108612. doi: 10.1016/j.

biopha.2019.108612.

- [38] Zhengfu H, Hu Z, Huiwen M, Zhijun L, Jiaojie Z, Xiaoyi Y, Xiujun C. 1-o-acetylbritannilactone (ABL) inhibits angiogenesis and lung cancer cell growth through regulating VEGF-Src-FAK signaling. *Biochem Biophys Res Commun*. 2015 Aug 21;464(2):422-7. doi: 10.1016/j.bbrc.2015.06.126.
- [39] Wang F, Li H, Qiao JO. 1-O-acetylbritannilactone combined with gemcitabine elicits growth inhibition and apoptosis in A549 human non-small cell lung cancer cells. *Mol Med Rep*. 2015 Oct;12(4):5568-72. doi: 10.3892/mmr.2015.4042.
- [40] Han YY, Tang JJ, Gao RF, Guo X, Lei M, Gao JM. A new semisynthetic 1-O-acetyl-6-O-lauroylbritannilactone induces apoptosis of human laryngocarcinoma cells through p53-dependent pathway. *Toxicol In Vitro*. 2016 Sep;35:112-20. doi: 10.1016/j.tiv.2016.05.019.
- [41] Huang LE, Cohen AL, Colman H, Jensen RL, Fuels DW, Couldwell WT. IGFBP2 expression predicts IDH-mutant glioma patient survival. *Oncotarget*. 2017 Jan 3;8(1):191-202. doi: 10.18632/oncotarget.13329.
- [42] Liu H, Weng J. A comprehensive bioinformatic analysis of cyclin-dependent kinase 2 (CDK2) in glioma. *Gene*. 2022 May 15;822:146325. doi: 10.1016/j.gene.2022.146325.
- [43] Yang L, Zeng W, Sun H, Huang F, Yang C, Cai X, Lu Y, Zeng J, Yang K. Bioinformatic Analysis of Gene Expression Omnibus Database Associates TAF7/CCNB1, TAF7/CCNA2, and GTF2E2/CDC20 Pathways with Glioblastoma Development and Prognosis. *World Neurosurg*. 2020 Jun;138:e492-e514. doi: 10.1016/j.wneu.2020.02.159.
- [44] Chen TC, Chuang JY, Ko CY, Kao TJ, Yang PY, Yu CH, Liu MS, Hu SL, Tsai YT, Chan H, Chang WC, Hsu TI. AR ubiquitination induced by the curcumin analog suppresses growth of temozolomide-resistant glioblastoma through disrupting GPX4-Mediated redox homeostasis. *Redox Biol*. 2020 Feb;30:101413. doi: 10.1016/j.redox.2019.101413.
- [45] Li M, Xu H, Qi Y, Pan Z, Li B, Gao Z, Zhao R, Xue H, Li G. Tumor-derived exosomes deliver the tumor suppressor miR-3591-3p to induce M2 macrophage polarization and promote glioma progression. *Oncogene*. 2022 Oct;41(41):4618-4632. doi: 10.1038/s41388-022-02457-w.
- [46] Xu P, Zhang G, Hou S, Sha LG. MAPK8 mediates resistance to temozolomide and apoptosis of glioblastoma cells through MAPK signaling pathway. *Biomed Pharmacother*. 2018 Oct;106:1419-1427. doi: 10.1016/j.biopha.2018.06.084.
- [47] Xu Y, Sun Q, Yuan F, Dong H, Zhang H, Geng R, Qi Y, Xiong X, Chen Q, Liu B. RND2 attenuates apoptosis and autophagy in glioblastoma cells by targeting the p38 MAPK signalling pathway. *J Exp Clin Cancer Res*. 2020 Aug 31;39(1):174. doi: 10.1186/s13046-020-01671-2.
- [48] Dunnett-Kane V, Burkitt-Wright E, Blackhall FH, Malliri A, Evans DG, Lindsay CR. Germline and sporadic cancers driven by the RAS pathway: parallels and contrasts. *Ann Oncol*. 2020 Jul;31(7):873-883. doi: 10.1016/j.annonc.2020.03.291.
- [49] Li X, Wu C, Chen N, Gu H, Yen A, Cao L, Wang E, Wang L. PI3K/Akt/mTOR signaling pathway and targeted therapy for glioblastoma. *Oncotarget*. 2016 May 31;7(22):33440-50. doi: 10.18632/oncotarget.7961.
- [50] Du Y, Li R, Fu D, Zhang B, Cui A, Shao Y, Lai Z, Chen R, Chen B, Wang Z, Zhang W, Chu L. Multi-omics technologies and molecular biomarkers in brain tumor-related epilepsy. *CNS Neurosci Ther*. 2024 Apr;30(4):e14717. doi: 10.1111/cns.14717.
- [51] Du Y, Wang H, Chen L, Fang Q, Zhang B, Jiang L, Wu Z, Yang Y, Zhou Y, Chen B, Lyu J, Wang Z. Non-RBM Mutations Impaired SARS-CoV-2 Spike Protein Regulated to the ACE2 Receptor Based on Molecular Dynamic Simulation. *Front Mol Biosci*. 2021 Jul 27;8:614443. doi: 10.3389/fmolb.2021.614443.